Individual Ion Activity Coefficients in Aqueous Electrolytes from Explicit-Water Molecular Dynamics Simulations

Sina Hassanjani Saravi and Athanassios Z. Panagiotopoulos*

Department of Chemical and Biological Engineering, Princeton University, Princeton, New Jersey 08544, USA

ABSTRACT

We compute individual ion activity coefficients (IIAC) in aqueous NaCl, KCl, NaF, and KF solutions from explicit-water molecular dynamics simulations. Free energy changes are obtained from insertion of single ions—accompanied by uniform neutralizing backgrounds—into solution by gradually turning on first Lennard-Jones interactions, followed by Coulombic interactions using Ewald electrostatics. Simulations are performed at multiple system sizes and all results are extrapolated to the thermodynamic limit, thus eliminating any possible artifacts from the neutralizing backgrounds. Due to controversies associated with measurements of IIAC from electrochemical cells with ion selective electrodes, the reported experimental data are not widely accepted, thus there remains a knowledge gap with respect to the contributions of individual ions to solution nonidealities. Our results are in good qualitative agreement with these reported measurements, though significantly larger in magnitude. Specifically, the relative positioning for the activity coefficients of anions and cations matches the experimental ordering for all four systems. The work establishes a robust thermodynamic framework, without a need to invoke extra hypotheses, that sheds light on the behavior of individual ions and their contributions to nonidealities of aqueous electrolyte solutions.

INTRODUCTION

Aqueous electrolyte solutions find widespread uses in diverse technological applications, and play key roles in many environmental[1, 2], biological[3, 4], and geological[5, 6] phenomena. While experiments provide direct measurements of key properties such as salt mean ionic activity coefficients and solubilities, modeling and simulation efforts have helped us gain significant knowledge on various characteristics of these complex fluids. Furthermore, such studies offer the opportunity of exploring extreme conditions under which experiments would be cumbersome if not impossible.

Molecular simulation approaches—whether in the form of molecular dynamics (MD) or Monte Carlo (MC)—have long been used to describe the behavior of aqueous electrolytes and quantify their thermodynamic and transport properties, over wide ranges of concentrations and temperatures[7-12]. Simulations of thermodynamic and transport properties, as well as nucleation rates of aqueous electrolytes have been recently reviewed[13]. While prior molecular simulation studies have offered us a fairly comprehensive picture of the behavior of aqueous salt solutions, there are few simulation studies on activity coefficients of individual ions. Analyzing the contributions to solution nonidealities for individual ions is of great interest for understanding the kinetics of homogeneous reactions[14], hydration thermodynamics[15, 16], electric double layer[16], and Donnan equilibria[17], to name a few. Furthermore, individual ions are important in biological systems[18] with a notable example being the Na^+/K^+-ATPase pump[19, 20].

One issue hindering broad development of a well-established framework to study and quantify individual ion activity coefficients (IIAC) has been the controversy around the experimental data reported in the literature. Measurements reported for IIAC—as opposed to mean ionic activity coefficients (MIAC)—are strongly debated, making them fall short of being a widely

accepted benchmark to which theoretical and simulation predictions could be compared. There have been significant efforts to design experimental methods for IIAC of 1:1 and 2:1 electrolytes[21-27]. These measurements are conducted in electrochemical cells consisting of ion selective electrodes (ISE) and reference electrodes, which entail electrical potential jumps at the interface of sample and reference solutions. The following relationship holds between the potentials for the cell, ion selective electrode, reference electrode, and liquid junction potential (LJP), denoted by $E, E_{\mathrm{ISE}}, E_{\mathrm{ref}}$ and E_{j}, respectively[25].

$$E = E_{\mathrm{ISE}} - E_{\mathrm{ref}} + E_{\mathrm{j}} \tag{1}$$

The equation can be rearranged as[25]

$$E - E_{\mathrm{j}} = E_0 + S \ln a_i \tag{2}$$

where E_0 is a combination of standard potential for the ISE electrode and the reference electrode potential, S is a general slope used in lieu of the Nernstian value (RT/z_iF), where R, T, z_i and F denote gas constant, temperature, the charge of single ion i, and Faraday constant, respectively; and a_i is the activity of single ion i. E_0 and S, both considered independent of concentration, are obtained by performing experiments at high dilution where the activity coefficient of single ions can be estimated from the Debye-Hückel limiting law. The hindrance however is that the LJP is not directly measurable and is interconnected with the activity coefficients of single ions. For this reason, Henderson's equation[28, 29], its modifications[30, 31], as well as a new analytical method[25] have been proposed as alternatives to link the LJP to ion transference numbers, which themselves are functions of molar conductivity. Several extra thermodynamic assumptions and strategies are then utilized to calculate analytically the LJP and subsequently the activity coefficients of single ions[25]. Other experimental studies in the literature reporting IIAC for symmetric and asymmetric aqueous electrolytes[32-38] have employed similar methodologies to obtain the LJP.

There are, however, discrepancies reported between data from different sources, even with respect to the relative positioning of IIAC for different ions. For instance, the Vera and Wilczek-Vera group showed[25] that the activity coefficients of Cl^- in KCl lie above those of K^+; an opposite trend compared to what was illustrated in NaCl. Measurements from Hurlen[32], on the other hand, show essentially no difference between the IIAC for K^+ and Cl^-; and data from Dash et al.[35] demonstrate the opposite trend, illustrating that the activity coefficients of K^+ are positioned above those of Cl^-. Valiskó and Boda[39] present a comparison between some of these data sets. The experimental measurements for IIAC have been strongly critiqued by Malatesta[40-44] and Zarubin[45-47]. They argued in several papers that due to the impossibility of directly measuring the LJP, the reported activity coefficients are the results of arbitrary conventions and alternate values could be obtained under different assumptions.

There have been a number of prior theoretical and simulation works that aim to obtain IIAC for aqueous electrolyte solutions. Theories employed for the calculation of IIAC include an extended version of Debye-Hückel (EDH)[48], hypernetted chain approximation (HNC)[49], mean spherical approximation (MSA)[14, 50], and symmetric Poisson-Boltzman[14], among others. Molecular simulation-based approaches, on the other hand, have been predominantly performed in implicit solvent, by utilizing variations of the primitive model (PM) for electrolytes in conjunction with MC simulations. The PM model considers ions as hard spheres placed in a dielectric continuum in lieu of explicit water molecules. Svensson and Woodward[51] utilized Widom's test particle method[52] to calculate chemical potentials and activity coefficients of individual ions for 1:1, 2:2, and 2:1 electrolytes, using this approach. Their method was later adopted by Lund et al.[53] for the activity coefficients in sea water. Sloth and Sørensen[49, 54, 55] employed PM models with ions of both equal and unequal sizes to calculate chemical potentials

and activity coefficients of single ions and compared results to the HNC approximation. Lamperski[56] reported calculations for MIAC and IIAC using PM models with grand-canonical Monte Carlo (GCMC). Malasics and Boda[57] later improved this approach using a faster-converging algorithm. Valiskó and Boda[39] calculated the IIAC by combining the contributions of ion-ion and ion-water interactions to the total excess chemical potentials. The ion-ion term was obtained from GCMC simulations with PM models using experimental Pauling radii, while the ion-water term was calculated from Born's treatment of solvation[58]. Furthermore, they considered a concentration-dependent ε_{r} with a polynomial function fitted to experimental data. In a more recent study, Abbas and Ahlberg[59] used MC simulations with PM to calculate IIAC and MIAC of several aqueous salts at elevated temperatures, with a concentration-dependent ε_{r}, adopted from Buchner et al.[60].

Although implicit-water simulations are computationally inexpensive, they do not include information on solution structure and ion hydration. Despite obtaining reasonable agreement between MIAC values from implicit-water simulations and experiments, they typically underestimate the chemical potentials by several orders of magnitude. By contrast, explicit-water simulations, do include information on the structure of solutions in the presence of water and circumvent the problems associated with assumptions about the concentration dependence of the relative permittivity, as ε_{r} is an outcome of the simulations. However, there have only been a few studies to date on activity coefficients or hydration free energies of individual ions from explicit-water simulations. Zhang et al.[61] presented the "(electro-)chemical potential difference" for Na^+, K^+, and Cl^- in aqueous NaCl and KCl solutions. This quantity is defined as a combination of chemical and electric contributions. The first contribution—in which we are most interested—is attributed to the activity of single ions whereas the second portion is due to a potential jump at the

water/air interface. The activity coefficients are calculated from a replica-exchange variation of thermodynamic integration method[62], using several combinations of force field parameters for ionic species and water models. The models investigated include AMBER[63], CHARM[64, 65], OPLS[66], and Dang95[67] for electrolytes in conjunction with SPC/E[68] and TIP3P[69] water models. Joung et al.[70], performed MD simulations for a number of alkali halide salts and calculated MIAC and solvation free energies at low salt concentrations, up to ~ 0.5 m, using the SPC/E[68] water model in conjunction with the Joung-Cheatham[63] force field for the ionic species.

Our focus in the present study is to develop a thermodynamically consistent framework to compute IIAC by simulation. These shed light on contributions of individual ions to solution nonideality, with particular interest to their relative positionings with respect to each other. The activity coefficients of individual ions for four aqueous alkali halide salts are obtained from explicit-water molecular dynamics simulations as the difference of the corresponding total chemical potential (μ_i) from an infinite dilution reference state ($\mu_i^\dagger$). The μ_i values are calculated from the Helmholtz free energy difference for insertion of a single ion into an aqueous salt solution. Such an insertion is carried out slowly by first placing a ghost particle into the solution, followed by turning on its Lennard-Jones and Coulombic interactions in stepwise manners. Full Ewald summations under periodic boundary conditions are performed for the electrostatic energy calculations and charge neutrality is achieved at all stages by a uniform countercharge to that of the added ion. We carry out multiple simulations at each concentration and extrapolate to infinite system size in order to eliminate any artifacts due to the uniform countercharge.

The rest of the article is organized as follows. In *Methods*, thermodynamics background, mathematical relations, and simulation details are discussed, and the framework is outlined in detail. In *Results and Discussion,* the simulation results are presented and comparisons are made

with experimental data, as well as with prior simulation predictions from the literature, followed by *Conclusions.* Furthermore, *Supporting Information* (SI) entails additional graphs and tables to complement the results and discussions.

METHODS

We select four aqueous electrolyte solutions, namely NaCl, KCl, NaF, and KF for the calculation of IIAC. MIAC values for these salts are available from prior molecular simulation studies in explicit water[63, 71-76]. For each salt, we perform simulations at several concentrations up to the experimental solubility limit at 298.15 K and 1 bar. A combination of SPC/E water model[68] and Joung and Cheatham (JC) force field parameters for ions[63] is used for the simulations, while the usual Lorentz-Berthelot combination rule is utilized for the cross interactions. While this model combination underestimates experimental solubilities[13], the degree of supersaturation at the experimental solubility limit is sufficiently small so that no artifacts from nucleation and precipitation of salt crystals are observed in any of the simulations. The chemical potential of individual ions (μ_i) in monovalent aqueous salts can be expressed by

$$\mu_i = \mu_i^\dagger + RT \ln m_i \gamma_i \tag{3}$$

where $\mu_i^\dagger$ is the Henry's law reference state chemical potential at infinite dilution; m_i is the concentration of the individual ion i in dimensionless molality, equal to that of salt in the case of monovalent solutions; and γ_i is the activity coefficient of ion i. Following Eq. 3, the activity coefficients of the individual ions can be calculated from the difference between the chemical potential at a finite concentration (μ_i) from that at the infinite dilution reference state ($\mu_i^\dagger$).

Mester and Panagiotopoulos[72, 77] previously showed that chemical potentials of aqueous salts can be calculated accurately from free energy difference for inserting a pair of ions into solution by gradually turning on their Lennard-Jones and electrostatic interactions. We undertake

a similar approach here with the difference that a single ion is inserted into solution in lieu of an ion pair. In principle, adding a single ion into solution will lead to a non-neutral simulation box. However, when using Ewald summations of electrostatic interactions under periodic boundary conditions, a uniform neutralizing background is included that renders the overall system electrically neutral. This added background charge does not exert any forces on the system charges and thus does not alter the dynamics of the ensemble[78]. In the thermodynamic limit, which is reached by extrapolating the simulation results to infinite system size, perturbations to the Hamiltonian of the system and hence any corresponding artifacts vanish. As a result, a thermodynamically feasible pathway can be established for the calculation of IIAC. This approach overcomes complications arising in the calculation of IIAC at the expense of additional computations to extrapolate the results to infinite system size. A number of other strategies previously undertaken in the literature to overcome such an issue include adding a correction term to the chemical potential obtained from standard Widom's test particle method[55], simple charge rescaling[51], and the multi-particle method in the GCMC approach[51].

At each concentration for a given salt, we consider separate sets of simulations, each containing a neutral solution with a specified number of water and salt molecules. A single cation or anion is then gradually inserted. The reference concentration for the IIAC thus obtained is considered to be the midpoint before and after insertion[79]. For instance, starting from a system containing 5 ion pairs and 5500 water molecules, the midpoint concentration is obtained as 5.5 salt "molecules" per 5500 water molecules, or 0.056 m, where m is the molality in mol salt / kg H_2O.

The chemical potential of the solution after adding a single ion i can be expressed as the summation of excess and ideal contributions:

$$\mu_i = \mu_i^{\mathrm{IG}} + \mu_i^{\mathrm{ex}} \tag{4}$$

The ideal gas chemical potential (μ_i^{IG}) can be obtained from

$$\mu_i^{\mathrm{IG}} = \mu_i^0 + \ln \frac{kTN}{P^0 \langle V \rangle} \tag{5}$$

where the standard chemical potential μ_i^0 is taken from the NIST-JANAF tables[80]; standard pressure is considered 1 bar; $\langle V \rangle$ denotes the average volume and N is the number of ion pairs obtained as the midpoint value before and after ion insertion. The excess chemical potential for adding a single ion from the ideal gas state into the solution can be obtained from the Helmholtz free energy difference as

$$\mu_i^{\mathrm{ex}} = \frac{\partial F}{\partial N} \approx \frac{\Delta F}{\Delta N} \tag{6}$$

Due to the strong electrostatic interactions, insertion of single ions is carried out slowly. Specifically, Lennard-Jones (LJ) and electrostatic interactions are expressed as functions of a coupling parameter (λ for LJ and ϕ for Coulombic), as in previous studies by Panagiotopoulos and coworkers[72, 77, 79, 81]. LJ interactions are turned on first with 21 windows with λ equally spaced in the range of [0,1]. While turning on LJ interactions, a soft-core "shifted" potential is applied to avoid discontinuity. These are then followed by gradually turning on the Coulombic interactions in 21 equally spaced windows in the ϕ parameter. The free energy difference in each step is obtained using Bennet's acceptance ratio (BAR)[77, 82]. The excess chemical potential is then calculated from

$$\mu_i^{\mathrm{ex}} = \sum_k \mu_{i,k}^{\mathrm{ex,LJ}} + \sum_k \mu_{i,k}^{\mathrm{ex,Coul}} \tag{7}$$

where $\mu_{i,k}^{\mathrm{ex,LJ}}$ and $\mu_{i,k}^{\mathrm{ex,Coul}}$ are excess chemical potentials for inserting the single ion i in the solution attributed to the LJ and Coulombic (Coul) interactions, respectively.

The uncertainties in excess chemical potentials are calculated from block averaging after initial NVT and NpT equilibrations, followed by discarding another 2 ns of the production runs. The final trajectories are divided into several uncorrelated blocks, over which the mean and standard errors specify the final quantities and associated uncertainties, respectively. We determine that blocks are uncorrelated by computing the autocorrelation function[83] for potential energies.

System size effects attributed to the implementation of Ewald summations under periodic boundary conditions have been studied by Young and Panagiotopoulos[79], who obtained a linear relationship of the chemical potentials with inverse simulation box length. Following this, we obtain the chemical potentials at the thermodynamic limit at each concentration, by carrying out simulations at multiple system sizes and extrapolating versus $1/L$:

$$\mu^{\mathrm{ex}}(L) = \frac{a}{L} + \mu^{\mathrm{ex}}(\infty) \tag{8}$$

The excess chemical potential at infinite size is then added to the ideal gas contribution, resulting in total chemical potential at the thermodynamic limit. The uncertainty for the excess chemical potential at infinite system size is calculated through instrumental weighting ($1/\sigma_i^2$), where σ_i is the standard error for each excess chemical potential data i. We report one standard deviation as the uncertainty associated with the intercept of a fitted line.

We use GROMACS version 2019.6[84] to carry out the MD simulations. At each window, we perform a 200 ps equilibration run in the NVT ensemble. This is then followed by a 2 ns NpT run using a leap-frog integrator at 298.15 K and 1 bar. Production runs are then performed with duration varying as per the number of particles in the simulation box, in the range of 10 – 40 ns. For the canonical and isothermal – isobaric ensembles at 298.15 K, the Nosé – Hoover thermostat[85, 86] is used with the coupling constant of 1 ps, and the time step for the MD runs are selected 2 fs. The cut-off for the Lennard-Jones interactions and the real space cut-off for the

electrostatic interactions are selected as 1 nm. Standard long-range corrections are used for the LJ interactions by assuming a homogeneous system beyond the cut-off distance with pair correlation function equal to unity. In the NpT ensemble, the Parrinello–Rahman barostat is used at a pressure of 1 bar with a coupling constant of 2 ps. Particle mesh Ewald summations are used for the electrostatic interactions with the Fourier-space grid of 0.1 nm, a sixth order interpolating function, and a relative tolerance of 1×10^{-6}.

Henry's law chemical potential is often calculated by replacing $\ln\gamma$ in Eq. 3 with an empirical expression, which itself is a function of molality. The result for the chemical potential at the lowest concentration, obtained from MD simulations, would then be fitted to Eq. 3 to calculate the $\mu_i^{\dagger}$. Such an approach has been pursued in previous studies with various empirical expressions, including among others, the Davies equation[87]. In the present study, we undertake two different approaches to obtain the reference state chemical potentials. The first approach is similar to the one described above but only considering the Debye-Hückel limit expression for the activity coefficients, in lieu of common empirical equations. The expression for chemical potential at infinite dilution can be rearranged as

$$\mu_i^{\dagger} = \mu_i - RT\ln m_i + ART\sqrt{m_i} \tag{9}$$

where the $\ln\gamma_i$ is replaced by $-A\sqrt{m_i}$ at infinite dilution limit; A is the Debye-Hückel parameter defined as

$$A = \frac{{q_e}^3\sqrt{2N_A\rho_s}}{8\pi(\varepsilon_r\varepsilon_0 k_b T)^{3/2}} \tag{10}$$

N_A is the Avogadro's number, ρ_s is the density of the solution, ε_0 is vacuum permittivity and ε_r is relative permittivity of the solution. Though the experimental value for the relative permittivity of water is 78.49[88], that of the SPC/E[68] water has been previously calculated[77] to be 73 and hence we

use the latter value to obtain the parameter A for consistency. Accordingly, the $\mu_i^\dagger$ can be obtained by inserting the simulation results for 0.019 m into Eq. 9. We refer to this approach as *enforcing the Debye-Hückel Slope* (DS).

In the second approach, we calculate $\mu_i^\dagger$ without enforcing the simulation results at infinite dilution to pass along the Debye-Hückel slope. One can rearrange the expression for excess chemical potential as

$$\mu^{ex} = (\mu^\dagger - \mu^\circ) + RT \ln m_i + RT \ln \gamma(m_i) - RT \ln \frac{NKT}{p^\circ \langle V \rangle} \tag{11}$$

At infinite dilution, the above equation can be reduced to

$$\mu^{ex} = (\mu^\dagger - \mu^\circ) - RT \ln \left(\frac{\rho_{\mathrm{H_2O}} RT}{p^\circ} \right) - ART\sqrt{m_i} \tag{12}$$

where $\rho_{\mathrm{H_2O}}$ is the density of pure SPC/E[68] water calculated in a system containing 5500 water molecules, and $\ln \gamma$ is replaced by $-A\sqrt{m_i}$ when approaching infinite dilution. Note that such an expression for $\ln \gamma$ is exact in the limit of infinitely high dilution. We can therefore establish a linear correlation between μ^{ex} and $\sqrt{m}$, from which $\mu^{ex,\infty}$ can be obtained by extrapolating a number of low-concentration simulation results to the limit of $\sqrt{m} \to 0$. As such, the y-intercept of the extrapolation gives the summation of the first two terms on the right-hand side of Eq. 12, from which $\mu^\dagger$ can be calculated. Since the chemical potentials that are extrapolated to infinite dilution have already been extrapolated to infinite system size, we refer to this approach as *Double Extrapolation* (DE).

RESULTS AND DISCUSSION

For each concentration, we run separate simulations for inserting a cation and an anion into solutions with 500, 1500, 2500, and 5500 water molecules with the number of salts varying as per

the concentration in molality. The exception is for the lowest concentration at 0.019 m, where we examine only three system sizes with 1500, 4500, and 7500 water molecules to avoid exceedingly demanding computations at the largest system size. The SPC/E[68]+ JC[63] model parameters used in our simulations are listed in Table S1 in the SI. A systematic study on the dependence of simulation results on various force fields is not within the scope of the current article. We will however demonstrate, by comparing our results to those in the literature, that such a dependence is unlikely to be significant.

Combining the chemical potentials calculated from insertion of a single cation and its counterion should be equivalent to the chemical potential corresponding to the insertion of a cation-anion pair. Figure S1 in SI shows the total chemical potentials obtained from combining the contributions of individual ions. Our simulation results match those reported by Mester and Panagiotopoulos[72, 77] using pair insertion, except for KF which was not investigated in the prior study. Although we later present a comprehensive analysis on the system size dependence of chemical potentials, we only show in this graph the results related to the smallest system sizes studied, i.e., 1500 water molecules for the lowest concentration and 500 for the rest. That is to be consistent with the study of Mester and Panagiotopoulos[72, 77] wherein they did not consider the system size effects. Numerical values for the chemical potentials are listed in Tables S2-S35 of the SI.

As discussed earlier, we extrapolate simulation data for the excess and total chemical potentials to infinite system size. One such example is shown in Figure 1 where the excess chemical potentials for adding a single Na^+ (top panel) and a single Cl^- (bottom panel) into separate NaCl solutions at 0.019 m are extrapolated versus inverse simulation box length to infinite system size. Numerical values for these two extrapolations are listed in Table S2 in the SI. As can be seen

from the table, μ^{ex} values for Na^+ and Cl^- in the thermodynamic limit illustrate a shift of, respectively, +0.78 and +0.97 kJ/mol when compared to the results at the lowest system size. These shifts translate to 0.31 to 0.39 difference in the calculated IIAC for these two ions, respectively, which is somewhat significant, thus establishing the need for the system size extrapolation. Tables S2-S35 in the SI contain details of all extrapolations to the thermodynamic limit for all four salts.

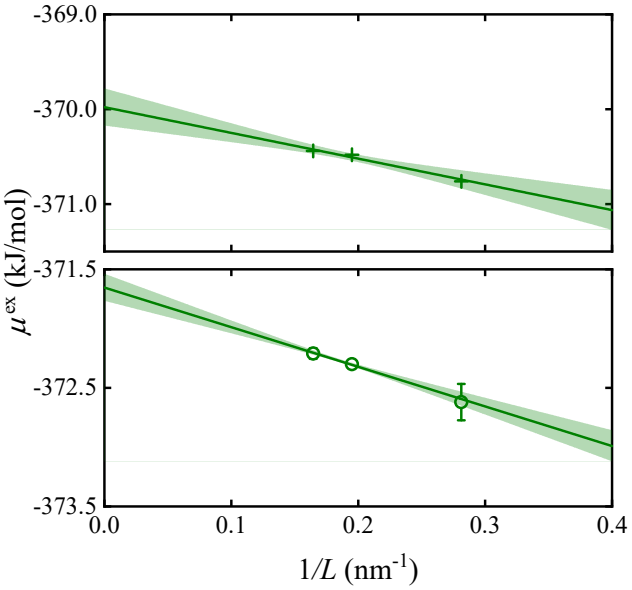

Figure 1. Extrapolation to infinite system size of simulation results for the excess chemical potentials, μ^{ex}, of adding a single Na^+ (top) and Cl^- (bottom) ion into aqueous NaCl solutions at overall salt concentration of 0.019 m. Solid lines represent linear fits and shadings denote one standard deviation for the fitted lines. Error bars are only shown when larger than the corresponding symbol size.

Figure 2 shows the excess chemical potentials versus square root of molality at 298.15 K and 1 bar. Each simulation point is the result of extrapolation to infinite system size as discussed above. The top and middle panels depict the contributions of LJ and Coulombic interactions, respectively, while the bottom panel shows the total excess chemical potential. The LJ portions ($\mu^{ex,LJ}$) demonstrate monotonic increases with increasing concentration, signifying that turning on these interactions between the inserted ion and solution species becomes relatively more unfavorable at higher concentrations. Furthermore, it can be seen that the magnitude of $\mu^{ex,LJ}$ is,

as expected, greater for larger species. It appears however that the LJ contribution for each single ion does not vary significantly from one aqueous solution to another. For instance, $\mu^{ex,LJ}$ values for Cl^- in NaCl versus KCl show almost no differences at low to moderate concentrations and exhibit only slight deviations at the highest molalities. The middle panel shows the Coulombic portion of the excess chemical potentials ($\mu^{ex,Coul}$) for ionic species in different aqueous solutions.

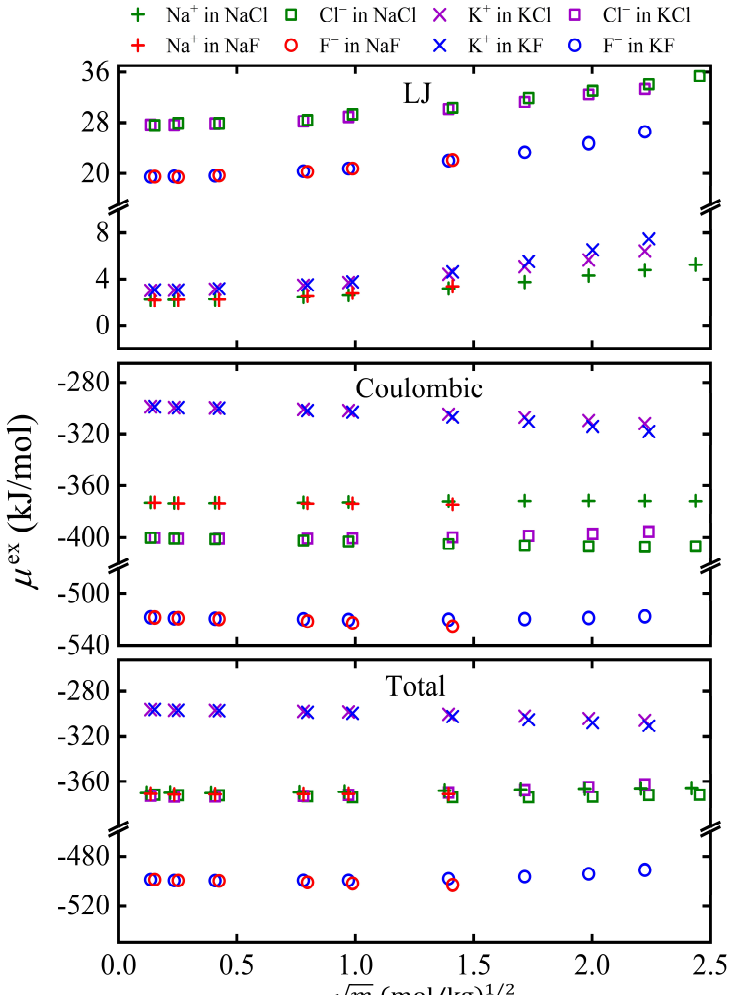

Figure 2. Simulation results for the excess chemical potentials, μ^{ex} (kJ/mol), of adding a single ion into aqueous solutions at 298.15 K and 1 bar versus $\sqrt{m}$, where m is the molality (mol salt / kg H_2O). **Top**: LJ contribution; **Middle**: Coulombic contribution; **Bottom**: total. Symbols denote ion types, Na^+ (+), Cl^- (□), K^+(×) , F^- (○). Colors denote the salt solution, NaCl (green), KCl (purple), NaF (red), and KF (blue). A slight horizontal offset is applied, when needed, to avoid overlapping symbols, in which case smaller x-values are the correct ones.

$\mu^{\mathrm{ex,Coul}}$ values for Cl^- are more negative compared to those for Na^+ and K^+. This indicates that the placement of Cl^- around water molecules is more favorable compared to Na^+ and K^+, despite the larger size of the anion. Between the two cations, K^+ displays—as anticipated—smaller negative contributions due to its lower charge density. In both aqueous NaCl and KCl solutions, $\mu^{\mathrm{ex,Coul}}$ values for Cl^- are the same up to ~2 m, elucidating the similarity of Coulombic interactions in the presence of various counterions at low concentrations. F^- exhibits the largest Coulombic contributions out of all the ions with a discernable difference in magnitude with $\mu^{\mathrm{ex,Coul}}$ for Cl^-, attributed to the smaller size of the F^- ion over Cl^-.

The bottom panel in Figure 2 depicts the total excess chemical potential (μ^{ex}) for individual ions versus $\sqrt{m}$, calculated by combining the LJ and Coulombic contributions. Due to the large scales of ordinate in the figure, changes in excess chemical potentials for each salt versus concentration are hard to distinguish, as the figure is rather meant to show the gaps between μ^{ex} quantities in different salts. The apparently small concentration dependence of μ^{ex} values still results in large changes when converted to MIAC and IIAC. Figure S2 in the SI demonstrates, as an example, the excess chemical potentials versus concentration for Na^+ and Cl^- in aqueous NaCl. As illustrated, insertion of a single Na^+ into solution becomes progressively less favorable with increasing concentration. On the other hand, such an insertion for Cl^- initially becomes more favorable with increasing concentration, before showing a minimum around 1.5 m, followed by an upward trend at higher concentrations.

It can be seen from Figure 2 that the gap between μ^{ex} for Na^+ and Cl^- in NaCl is much narrower compared to that between K^+ and Cl^- in KCl. Furthermore, K^+ is showing smaller negative values for μ^{ex} compared to Na^+, signifying that solvation of the former cation is relatively more unfavorable in water compared to the latter. We may thus deduce that the gaps between μ^{ex}

for Na^+ and Cl^- are smaller than those between K^+ and Cl^-, as the former cation has a tendency toward hydration, while the latter is more drawn toward its counterion rather than water. Further analysis of radial distribution functions (RDFs) for the pair of anion-cation in the two aqueous solutions also confirms this argument. As shown in Figure 3, the pair correlation function of Na^+–Cl^- (top panel) demonstrates a smaller first peak, known as the contact ion pair (CIP), followed by a larger second peak, illustrating the solvent separated ion pair (SSIP). In the RDF of K^+–Cl^- (bottom panel), there exists a pronounced first peak (CIP)—interpreted as stronger "ion association"—followed by a smaller second (SSIP) peak, as opposed to the NaCl solution where SSIP configurations are dominant[9]. These observations are consistent with prior simulation results in the literature[9, 77], some of which have been performed with different combination of force fields. These confirm that the cation in NaCl has a hydration tendency, while insertion of Cl^- is even more favorable. Thus, the gaps between the excess chemical potentials of the cation and anion are relatively low. In KCl, on the other hand, due to strong ion association, the cation is more drawn to its counterion rather to water. The cation therefore has less tendency to be placed near water molecules which leads to lower negative numbers for the corresponding μ^{ex}. As such, one expects larger gaps between excess chemical potentials of K^+ and Cl^- in KCl. Finally, we observe that the gaps between μ^{ex} of the anion and cation in KF are larger than those in NaF, similar to the trends previously illustrated for KF versus KCl. It must however be noted that the correlation between the gaps and liquid microstructure may be force field dependent. As such, systematic analyses are needed with various force fields to draw a more certain conclusion, which would be the subject of future studies.

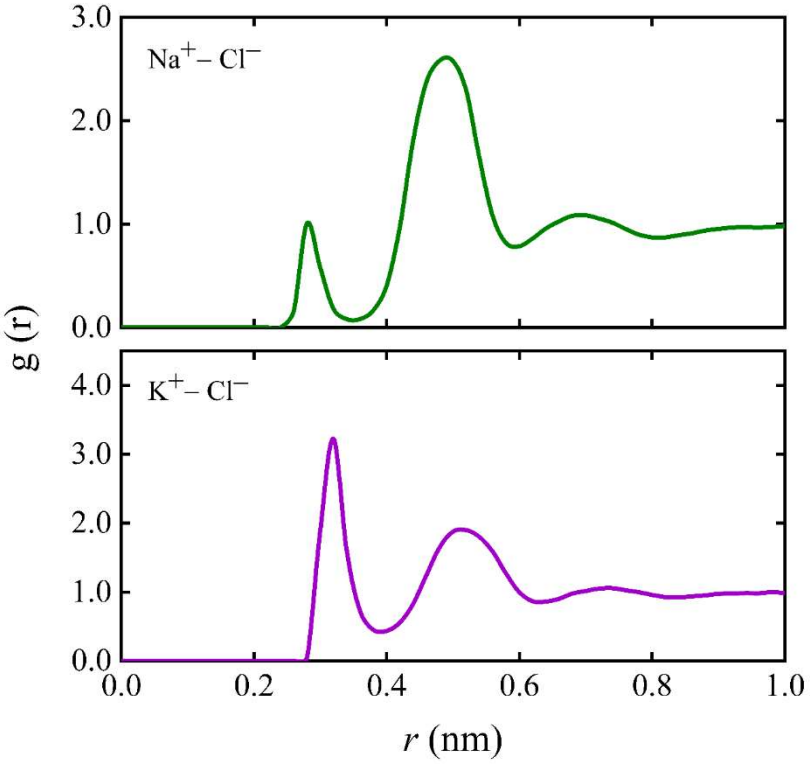

Figure 3. Pair correlation function, g (r), of Na^+ – Cl^- (top panel) and K^+ – Cl^- (bottom panel) in aqueous NaCl and KCl, respectively, both at salt concentration of 4.9 m.

The reference state chemical potentials ($\mu_i^\dagger$) are obtained from two separate approaches, DS and DE, as explained earlier. Both values are listed in Tables S36-S39 of the SI. Note that in the second approach (DE), the chemical potentials at the three lowest concentrations—0.019, 0.056, and 0.167 m—are extrapolated linearly versus $\sqrt{m}$ to infinite dilution. Figure S3 of the SI demonstrates, as an example, two such extrapolations to infinite dilution for Na^+ and Cl^- in aqueous NaCl. From this point onwards, we only present and discuss IIAC and MIAC results using the DS method, which provides more accuracy. We first discuss the results for MIAC, since values are available in the literature and the pertinent experimental data are well established. Figure 4 shows the MIAC values, calculated from the contributions of individual ions, versus $\sqrt{m}$ for the four solutions studied. Our calculated MIAC values almost match perfectly with those reported by Young and Panagiotopoulos[79] using a pair insertion method, with both studies taking into account

the system size effects – these earlier results are not shown in the figure for clarity. Mester and Panagiotopoulos[77], on the other hand, did not extrapolate results to infinite system size; however, their predictions are still in good agreement with this work within the statistical uncertainties, as shown in the figure. Simulation results for all four salts compare reasonably well with the experimental data of Robinson and Stokes[89] at low concentrations before deviating at higher concentrations. This is attributed to the limitations associated with classical non-polarizable force fields, as also observed in prior works[72, 77, 79, 81].

Having established that our approach, based on calculations for individual ions, gives overall activity coefficients (MIAC) in agreement to literature values, we now turn our attention to the activity coefficients of the individual ions (IIAC). Figure 5 shows our results and compares them to experimental data and prior simulations for other models. The top panel of Figure 5 shows the experimental data of Vera and Wilczek-Vera group[25] fitted to polynomial functions. Simulation results from the present study are shown in middle panel and those reported by Zhang et al.[61] are shown in the bottom panel. As can be seen from our simulation results, the gaps between IIAC of Na^+ and Cl^- are narrower whereas such gaps are larger between those of the cation and anion in KCl. Similarly, we observe that there is a significant gap between IIAC of K^+ and F^- in KF, as opposed to NaF where such gaps are shown to be narrower. From these behaviors—consistent with our previous arguments for excess chemical potentials—one may arrive at a similar interpretation that in salts with higher tendency for ion hydration, the gaps between the IIAC of anions and cations become narrower, whereas in solutions with stronger ion association, such gaps will render larger.

Furthermore, our simulation results for activity coefficients of Na^+ in NaCl solutions show positive deviations from the ideal solution, as opposed to those of Cl^-, which display negative

deviations. The relative order, Cl^- below Na^+, signifies that the anion has more favorable interactions in aqueous NaCl solutions at high concentrations. The simulation results are in qualitative agreement with the experimental data[25] illustrated in the top panel, in terms of the positioning of IIAC with respect to each other in all four salts. In other words, the activity coefficients of cations from both experiments and our explicit-water simulations are shown to be positioned above those of anions in NaCl and NaF, while such orders are reverse in KCl and KF. The magnitude of the activity coefficients from simulations are however up to factors of two to three larger than those from experiments. These discrepancies could be attributed to both the arbitrary analytical treatment of LJP in experiments—as discussed earlier—and the possible effects of artifacts in simulations. Also, it should be noted that deviations of simulation results at higher concentrations are in part related to the poor performance of the force field parameters employed, as seen previously for MIAC in Figure 4.

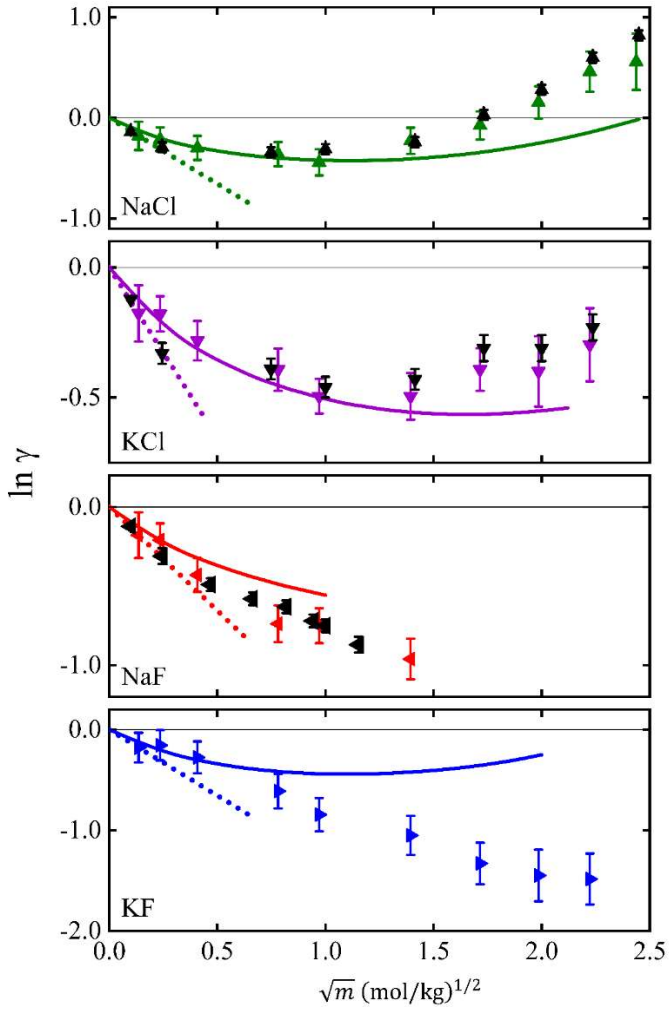

Figure 4. Mean ionic activity coefficients in aqueous NaCl, KCl, NaF, and KF solutions at 298.15 K and 1 bar versus $\sqrt{m}$, where m is the molality (mol salt / kg H_2O). Solid lines represent experimental data from[89]; dotted lines are the Debye-Hückel limiting slope. Simulation results from the present study are shown by colored triangles for NaCl (green), KCl (purple), NaF (red), and KF (blue). Black triangles denote prior simulation results from Mester and Panagiotopoulos[72, 77].

The orders for activity coefficients of the cation and anion in KCl are reverse relative to NaCl, indicating more favorable interactions for cation compared to the anion in KCl solutions. Similar trends are observed in aqueous KF where the activity coefficients of anions are positioned above those of cations. On the other hand, in NaF, the activity coefficients of Na^+ lie above those of F^-. Finally, in both KCl and KF the IIAC for K^+ are positioned below those of anions, as opposed to the trends observed in NaCl and NaF.

These results reveal the subtle effects of solution structure on the ordering of IIAC in different salts. As such, one cannot easily predict the relative positioning of IIAC of anions and cations without conducting explicit-water simulations. Evidence for that includes limitations—and failure in some cases—of phenomenological models in predicting the correct positionings. There are several proposed such models in the literature that break down the intermolecular interactions into several additive contributions of different "physical" origins.

In a recent study, Sun et al.[90] have laid out several of these models and applied them to calculate the IIAC in a number of mono- and multi-valent aqueous electrolytes. For the ion-ion interactions, Sun et al[90] utilized three different approaches, including electrolyte cubic plus association (e-CPA)[91], EDH[92], and MSA[93]. The Born treatment[58] of solvation was used for the ion-water interactions. Among the aqueous solutions investigated, three in particular are of interest for the present study including NaCl, KCl, and NaF. For example, in aqueous NaCl, the MSA + Born approach shows essentially no differences in quantities for the IIAC of Na^+ and Cl^-. On the other hand, the e-CPA—i.e., Debye-Hückel (DH) + Born—shows that the IIAC of Cl^- are positioned above those of Na^+. Finally, EDH + Born returns correct trends, showing that the IIAC of Na^+ lie above those of Cl^-.

In KCl, EDH + Born produces wrong orders for the IIAC of K^+ and Cl^-, while e-CPA predicts essentially the same values of IIAC for both ions. MSA + Born returns correct trends, however, with almost no distinction between the values for IIAC of K^+ and Cl^-. Finally, in NaF, while EDH + Born results in almost no differences in values for IIAC of Na^+ and F^-, the other two approaches produce wrong trends. These inconsistencies underscore the shortcomings associated with models that do not explicitly account for the water molecules. In the absence of proper liquid

structure, one cannot correctly predict the contributions of individual ions to solution nonideality, and therefore correct orders for IIAC.

As mentioned previously, Zhang et al.[61] presented activity coefficients of Cl^- in aqueous NaCl and KCl using several force field combinations. As demonstrated in the bottom panel in Figure 5, the activity coefficients of Cl^- calculated by these authors using SPC/E[68]+AMBER[63] and TIP3P[69]+AMBER[63] are in good agreement with our simulation results. This confirms larger magnitudes for the activity coefficients of individual ions from explicit-water simulations compared to those obtained from the PM+MC approaches. Note that the "AMBER" model for ions used in the study of Zhang et al.[61] is the same as "JC". We kept their annotation "as-is" to follow the original notation. We further calculated $\Delta\mu^{\mathrm{ex}}$ in NaCl—defined as $\mu^{\mathrm{ex}} - \mu^{\mathrm{ex},\infty}$ in the article published by Joung et al.[70]—in order to make another comparison of our results with explicit-water simulations in the literature. Our results agree reasonably well with the prior calculations, with a notable difference being the excess chemical potential of individual ions at infinite dilution. In the present study, we obtain $\mu_{\mathrm{Na}^+}^{\mathrm{ex},\infty}$ and $\mu_{\mathrm{Cl}^-}^{\mathrm{ex},\infty}$ separately from the double extrapolation method— as -369.69 ± 0.14 and -371.66 ± 0.25 kJ/mol, respectively—while the prior study simply allocated half of the total excess chemical potential, calculated from the Debye-Hückel theory to each ion.

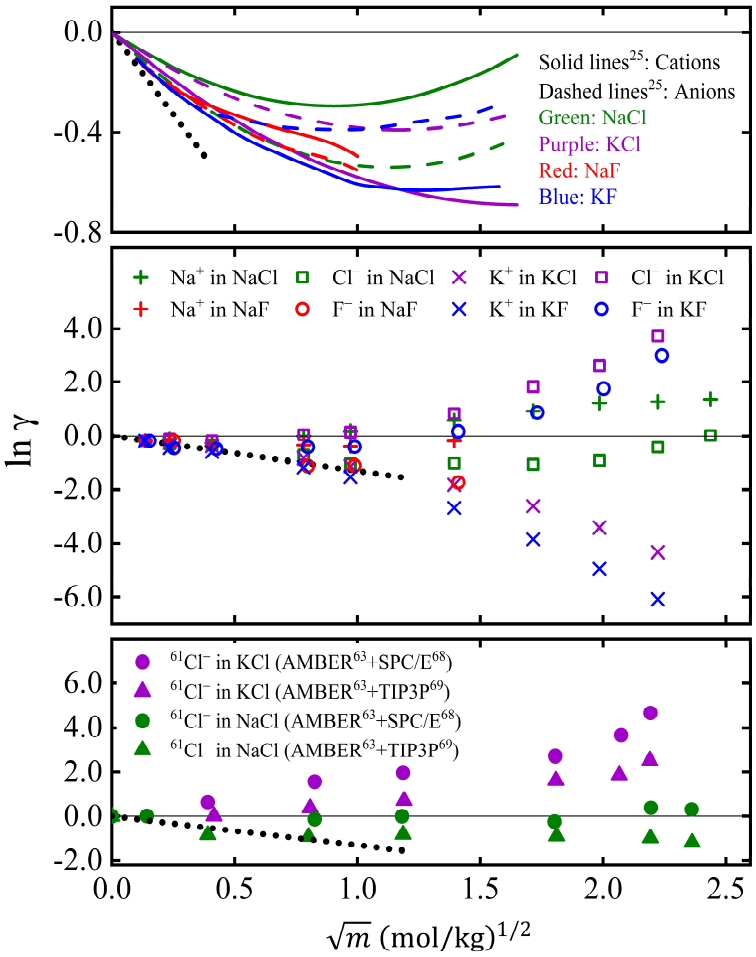

Figure 5. Individual ion activity coefficients in aqueous solutions at 298.15 K and 1 bar versus $\sqrt{m}$, where m is the molality (mol salt / kg H_2O). **Top**: Experimental data from[25] fitted to polynomials. Solid and dashed lines represent the cations and anions, respectively, while colors denote the salt solution, NaCl (green), KCl (purple), NaF (red), and KF (blue). **Middle**: Simulation results from this study with symbols denoting ion types, Na^+ (+), Cl^- (□), K^+(×) , F^- (○), following the same color code as for the top graph. **Bottom**: Simulation results from Zhang et al.[61] for $\ln \gamma_{Cl^-}$: green and purple filled circles denote results in NaCl and KCl, respectively, with SPC/E[68]+AMBER[63]; green and purple filled triangles show results in NaCl and KCl, respectively, with TIP3P[69]+AMBER[63]. Short-dotted lines represent the Debye-Hückel limiting slope.

CONCLUSIONS

In this article, we obtained individual ion activity coefficients (IIAC) in several aqueous electrolyte solutions, namely NaCl, KCl, NaF, and KF, with explicit-water molecular dynamics simulations. Chemical potentials at each concentration were calculated from free energy change for insertion of a single ion into aqueous solution. We use the "slow growth" method and Bennet's

acceptance ratio to obtain the free energy change by gradually turning on the Lennard-Jones and Coulombic interactions—in stepwise manners—between the inserted ion and solution constituents. The infinite dilution reference state ($\mu_i^\dagger$) was obtained using two approaches: one, by enforcing the simulation results at the lowest concentration studied to pass along the Debye-Hückel limiting slope, and the other by extrapolating the chemical potentials at several low concentrations to infinite dilution. The first approach, not surprisingly, results in more accurate $\mu_i^\dagger$ values. The second approach—though entirely predictive without considering any extra parameters—results in satisfactory estimations for $\mu_i^\dagger$, with larger uncertainties which in turn would propagate to significant errors for the activity coefficients.

Chemical potentials calculated from combining the contributions of individual ions agree well with those previously obtained from pair insertion method. This agreement demonstrates the consistency of the thermodynamic framework of the present study. Furthermore, breaking down the total excess chemical potentials into Lennard-Jones and Coulombic contributions elucidates the effects of physical forces of different nature on the overall nonideality of the solution.

We compared the simulation IIAC results to reported experimental data, measured through electrochemical cells with ion selective electrodes, which are controversial due to several extra thermodynamic hypotheses employed to obtain them from the raw experimental measurements. Our simulation results are in qualitative agreement with the experimental data with respect to the relative positioning of IIAC of ions, however, they have significantly larger magnitudes. Such larger values for the activity coefficients of individual ions from explicit-water simulations have been previously observed in the literature. We show that the activity coefficients of individual ions strongly depend on solution structure in the presence of different counterions. One such example is the contribution of Cl^- to solution nonideality in aqueous NaCl versus KCl. While the activity

coefficients of Cl^- show negative deviations in the former solution, they illustrate large positive deviations in the latter aqueous salt. It appears that in solutions with more tendency for ion hydration, the gaps between IIAC for anions and cations become narrower. In aqueous salts with stronger "ion association", on the other hand, such gaps would turn out to be larger and deviations from ideal solution become amplified. Tighter gaps are observed between the activity coefficients of anions and cations in NaF and NaCl, compared to KF and KCl. Furthermore, we observe in NaCl and NaF that the activity coefficients of Na^+ lie above those for Cl^- and F^-, respectively, whereas in KCl and KF, the IIAC for both anions lie above the activity coefficient of K^+.

There are significant challenges in predicting the correct trends for IIAC of cations and anions in electrolyte solutions, when using phenomenological models, as demonstrated previously in the literature. Expressing the intermolecular interactions as combinations of different additive contributions leads to different orders in the activity coefficients, often resulting in disagreements with experimental data. Somewhat surprisingly, simulations using existing ion and water force fields in explicit-water simulations, without any adjustment of interaction parameters, are shown here to be able to obtain the correct ordering of the IIAC.

More broadly, this work establishes a sound thermodynamic framework to describe the behavior of individual ions from an atomistic point of view and portrays their unequal contributions to solution nonideality. Future work could be directed toward complementing the current approach by conducting systematic investigations on the temperature dependence of individual ion activity coefficients, as well as pursuing calculations of IIAC in aqueous solutions of mixed salts and mixed-solvent electrolytes.

We are currently undertaking a separate study wherein calculations of IIAC are pursued using implicit-water simulations with concentration-dependent relative permittivity. Such a study

will provide a framework to compare the implicit- and explicit-water simulations in predicting IIAC, and casts light on the ability of these two approaches in quantifying the thermodynamic and transport properties of individual ions in various aqueous electrolyte solutions.

ASSOCIATED CONTENT

Supporting Information (SI)

SI includes figures for total chemical potentials versus concentration and extrapolation of chemical potentials to infinite dilution, tables for model parameters for force fields used, chemical potentials, and individual and mean ionic activity coefficients.

AUTHOR INFORMATION

Corresponding Author

*E-mail: azp@princeton.edu.

ORCID

Sina Hassanjani Saravi: https://orcid.org/0000-0002-8257-1266

Athanassios Z. Panagiotopoulos: https://orcid.org/0000-0002-8152-6615

Notes

The authors declare no competing financial interest.

ACKNOWLEDGMENTS

The authors wish to thank the European Research Council (ERC) for funding this research under the European Union's Horizon 2020 research and innovation program (Grant Agreement No. 832460), ERC Advanced Grant project "New Paradigm in Electrolyte Thermodynamics". Additional support was provided by the Princeton Center for Complex Materials, a US National

Science Foundation Materials Research Science and Engineering Center (Award No. DMR-1420541). Simulations were performed using computational resources supported by the Princeton Institute for Computational Science and Engineering (PICSciE) and the Office of Information Technology's High Performance Computing Center at Princeton University.

REFERENCES

1. Honarparvar, S.; Zhang, X.; Chen, T.; Na, C.; Reible, D. Modeling technologies for desalination of brackish water—toward a sustainable water supply. *Curr. Opin. Chem. Eng.* **2019,** *26*, 104-111.

2. Honarparvar, S.; Zhang, X.; Chen, T.; Alborzi, A.; Afroz, K.; Reible, D. Frontiers of membrane desalination processes for brackish water treatment: A review. *Membranes* **2021,** *11*, 246.

3. Arrigan, D. W.; Hackett, M. J.; Mancera, R. L. Electrochemistry of proteins at the interface between two immiscible electrolyte solutions. *Curr. Opin. Electrochem.* **2018,** *12*, 27-32.

4. Hess, B.; van der Vegt, N. F. Cation specific binding with protein surface charges. *Proc. Natl. Acad. Sci. U. S. A.* **2009,** *106*, 13296-13300.

5. Rowan, E.; Engle, M.; Kirby, C.; Kraemer, T. Radium content of oil-and gas-field produced waters in the Northern Appalachian Basin (USA): Summary and discussion of data. *US Geological Survey Scientific Investigations Report* **2011,** *5135*, 31.

6. Zheng, R.; Fan, Z.; Li, X.; Negahban, S. Phase behavior of high-pressure CH_4-CO_2 hydrates in NaCl solutions. *Fuel* **2020,** *280*, 118549.

7. Degrève, L.; Lozada-Cassou, M.; Sánchez, E.; González-Tovar, E. Monte Carlo simulation for a symmetrical electrolyte next to a charged spherical colloid particle. *J. Chem. Phys.* **1993,** *98*, 8905-8909.

8. Lyubartsev, A. P.; Laaksonen, A. Concentration effects in aqueous NaCl solutions. A molecular dynamics simulation. *J. Phys. Chem.* **1996,** *100*, 16410-16418.

9. Chowdhuri, S.; Chandra, A. Molecular dynamics simulations of aqueous NaCl and KCl solutions: Effects of ion concentration on the single-particle, pair, and collective dynamical properties of ions and water molecules. *J. Chem. Phys.* **2001,** *115*, 3732-3741.

10. Boda, D. Monte Carlo simulation of electrolyte solutions in biology: In and out of equilibrium. In *Annu. Rep. Comput. Chem.*, Elsevier: 2014; Vol. 10, pp 127-163.

11. Nezbeda, I.; Moučka, F.; Smith, W. R. Recent progress in molecular simulation of aqueous electrolytes: Force fields, chemical potentials and solubility. *Mol. Phys.* **2016,** *114*, 1665-1690.

12. Smith, W. R.; Nezbeda, I.; Kolafa, J.; Moučka, F. Recent progress in the molecular simulation of thermodynamic properties of aqueous electrolyte solutions. *Fluid Phase Equilib.* **2018,** *466*, 19-30.

13. Panagiotopoulos, A. Z. Simulations of activities, solubilities, transport properties, and nucleation rates for aqueous electrolyte solutions. *J. Chem. Phys.* **2020,** *153*, 010903.

14. Molero, M.; Outhwaite, C. W.; Bhuiyan, L. B. Individual ionic activity coefficients from a symmetric Poisson–Boltzmann theory. *J. Chem. Soc., Faraday Trans.* **1992,** *88*, 1541-1547.

15. Zhou, J.; Lu, X.; Wang, Y.; Shi, J. Molecular dynamics study on ionic hydration. *Fluid Phase Equilib.* **2002,** *194*, 257-270.

16. Vlcek, L.; Chialvo, A. A. Single-ion hydration thermodynamics from clusters to bulk solutions: Recent insights from molecular modeling. *Fluid Phase Equilib.* **2016,** *407*, 58-75.

17. Honarparvar, S.; Reible, D. Modeling multicomponent ion transport to investigate selective ion removal in electrodialysis. *Environmental Science and Ecotechnology* **2020,** *1*, 100007.

18. Kunz, W. Specific ion effects in colloidal and biological systems. *Curr. Opin. Colloid Interface Sci.* **2010,** *15*, 34-39.

19. Skou, J. C. The identification of the sodium pump. *Biosci. Rep.* **1998,** *18*, 155-169.

20. Pirahanchi, Y.; Aeddula, N. Physiology, Sodium Potassium Pump (Na+ K+ Pump)[Updated 2019 Jan 21]. *StatPearls [Internet]. Treasure Island, FL: StatPearls Publishing* **2020**.

21. Khoshkbarchi, M. K.; Vera, J. H. Measurement and correlation of ion activity in aqueous single electrolyte solutions. *AIChE J.* **1996,** *42*, 249-258.

22. Taghikhani, V.; Modarress, H.; Vera, J. H. Individual anionic activity coefficients in aqueous electrolyte solutions of LiCl and LiBr. *Fluid Phase Equilib.* **1999,** *166*, 67-77.

23. Taghikhani, V.; Vera, J. H.; Modarress, H. Measurement and correlation of the individual ionic activity coefficients of aqueous electrolyte solutions of KF, NaF and KBr. *Can J Chem Eng* **2000,** *78*, 175-181.

24. Rodil, E.; Vera, J. Individual activity coefficients of chloride ions in aqueous solutions of $MgCl_2$, $CaCl_2$ and $BaCl_2$ at 298.2 K. *Fluid Phase Equilib.* **2001,** *187*, 15-27.

25. Wilczek-Vera, G.; Rodil, E.; Vera, J. H. On the activity of ions and the junction potential: Revised values for all data. *AIChE J.* **2004,** *50*, 445-462.

26. Wilczek-Vera, G.; Vera, J. H. On the measurement of individual ion activities. *Fluid Phase Equilib.* **2005,** *236*, 96-110.

27. Wilczek-Vera, G.; Vera, J. H. How much do we know about the activity of individual ions? *J. Chem. Thermodyn.* **2016,** *99*, 65-69.

28. Henderson, P., *Zur thermodynamik der flüssigkeitsketten*. Druck von WF Kaestner: 1907.

29. Henderson, F. Zur thermodynamik der flüssigkeitsketten. *Z. Phys. Chem.* **1908,** *63*, 325-345.

30. Harned, H. S. Individual thermodynamic behaviors of ions in concentrated solutions including a discussion of the thermodynamic method of computing liquid-junction potentials. *J. Phys. Chem.* **2002,** *30*, 433-456.

31. Harper, H. W. Calculation of liquid junction potentials. *J. Phys. Chem.* **1985,** *89*, 1659-1664.

32. Hurlen, T. Convenient single-ion activities. *Acta Chem Scand A* **1979,** *33*, 631-635.

33. Hurlen, T. Ion activities of alkaline-earth chlorides in aqueous-solution. *Acta Chem Scand A* **1979,** *33*, 637-640.

34. Hurlen, T.; Breivik, T. R. Ion activities of alkali-metal bromides in aqueous-solution. *Acta Chem Scand A* **1981,** *35*, 415-418.

35. Dash, D.; Kumar, S.; Mallika, C.; Mudali, U. K. New data on activity coefficients of potassium, nitrate, and chloride ions in aqueous solutions of KNO_3 and KCl by ion selective electrodes. *Int. Scholarly Res. Not.* **2012,** *2012*.

36. Lee, L.-S.; Chen, T.-M.; Tsai, K.-M.; Lin, C.-L. Individual ion and mean activity coefficients in NaCl, NaBr, KCl and KBr aqueous solutions. *J. Chin. Inst. Chem. Eng.* **2002,** *33*, 267-281.

37. Zhuo, K.; Dong, W.; Wang, W.; Wang, J. Activity coefficients of individual ions in aqueous solutions of sodium halides at 298.15 K. *Fluid Phase Equilib.* **2008,** *274*, 80-84.

38. Shatkay, A.; Lerman, A. Individual activities of sodium and chloride ions in aqueous solutions of sodium chloride. *Anal. Chem.* **1969,** *41*, 514-517.

39. Valiskó, M.; Boda, D. Unraveling the behavior of the individual ionic activity coefficients on the basis of the balance of ion–ion and ion–water interactions. *J. Phys. Chem. B* **2015,** *119*, 1546-1557.

40. Malatesta, F. The impossibility of measuring individual ion activity coefficients using ion selective electrodes. *J. Solution Chem.* **2000,** *29*, 771-779.

41. Malatesta, F. On the Rodil–Vera method for determining ion activity coefficients. *Fluid Phase Equilib.* **2005,** *233*, 103-109.

42. Malatesta, F. On the experimental determinations of ionic activity coefficients. *Fluid Phase Equilib.* **2006,** *239*, 120-124.

43. Malatesta, F. Activity coefficients of ions in sodium halide solutions: Critical remarks. *Fluid Phase Equilib.* **2010,** *295*, 244-248.

44. Malatesta, F. Comment on the individual ion activities of Na^+ and Cl^- by Arce, Wilczek-Vera and Vera. *Chem. Eng. Sci.* **2010,** *65*, 675-679.

45. Zarubin, D. P. The nature of single-ion activity coefficients calculated from potentiometric measurements on cells with liquid junctions. *J. Chem. Thermodyn.* **2011,** *43*, 1135-1152.

46. Zarubin, D. P. Reply to comment by JH Vera and G. Wilczek-Vera on'The nature of single-ion activity coefficients calculated from potentiometric measurements on cells with liquid junctions'. *J. Chem. Thermodyn.* **2012,** *47*, 445-448.

47. Zarubin, D. P. The debate with G. Wilczek-Vera and JH Vera. *J. Chem. Thermodyn.* **2012,** 451-452.

48. Ritsema, C. Estimation of activity coefficients of individual ions in solutions with ionic strengths up to 0.3 mol dm^{-3}. *J. Soil Sci.* **1993,** *44*, 307-315.

49. Sloth, P.; Sørensen, T. S. Single-ion activity coefficients and structure of ionic fluids: results for the primitive model of electrolyte solutions. *J. Phys. Chem.* **1990,** *94*, 2116-2123.

50. Taghikhani, V.; Modarress, H.; Khoshkbarchi, M. K.; Vera, J. H. Application of the MSA to the modeling of the activity coefficients of individual ions. *Fluid Phase Equilib.* **2000,** *167*, 161-171.

51. Svensson, B. R.; Woodward, C. E. Widom's method for uniform and non-uniform electrolyte solutions. *Mol. Phys.* **1988,** *64*, 247-259.

52. Widom, B. Some topics in the theory of fluids. *J. Chem. Phys.* **1963,** *39*, 2808-2812.

53. Lund, M.; Jönsson, B.; Pedersen, T. Activity coefficients in sea water using Monte Carlo simulations. *Mar. Chem.* **2003,** *80*, 95-101.

54. Sloth, P.; Sørensen, T. S. Monte Carlo simulations of single ion chemical potentials. Results for the unrestricted primitive model. *Chem. Phys. Lett.* **1988,** *146*, 452-455.

55. Sloth, P.; Sørensen, T. S. Monte Carlo calculations of chemical potentials in ionic fluids by application of Widom's formula: Correction for finite-system effects. *Chem. Phys. Lett.* **1990,** *173*, 51-56.

56. Lamperski, S. The individual and mean activity coefficients of an electrolyte from the inverse GCMC simulation. *Mol. Simul.* **2007,** *33*, 1193-1198.

57. Malasics, A.; Boda, D. An efficient iterative grand canonical Monte Carlo algorithm to determine individual ionic chemical potentials in electrolytes. *J. Chem. Phys.* **2010,** *132*, 244103.

58. Born, M. Volumen und hydratationswärme der ionen. *Z. Phys.* **1920,** *1*, 45-48.

59. Abbas, Z.; Ahlberg, E. Activity coefficients of concentrated salt solutions: A Monte Carlo investigation. *J. Solution Chem.* **2019,** *48*, 1222-1243.

60. Buchner, R.; Hefter, G. T.; May, P. M. Dielectric relaxation of aqueous NaCl solutions. *J. Phys. Chem. A* **1999,** *103*, 1-9.

61. Zhang, C.; Raugei, S.; Eisenberg, B.; Carloni, P. Molecular dynamics in physiological solutions: force fields, alkali metal ions, and ionic strength. *J. Chem. Theory Comput.* **2010,** *6*, 2167-2175.

62. Fukunishi, H.; Watanabe, O.; Takada, S. On the Hamiltonian replica exchange method for efficient sampling of biomolecular systems: Application to protein structure prediction. *J. Chem. Phys.* **2002,** *116*, 9058-9067.

63. Joung, I. S.; Cheatham III, T. E. Determination of alkali and halide monovalent ion parameters for use in explicitly solvated biomolecular simulations. *J. Phys. Chem. B* **2008,** *112*, 9020-9041.

64. Beglov, D.; Roux, B. Finite representation of an infinite bulk system: solvent boundary potential for computer simulations. *J. Chem. Phys.* **1994,** *100*, 9050-9063.

65. Roux, B. Valence selectivity of the gramicidin channel: a molecular dynamics free energy perturbation study. *Biophys. J.* **1996,** *71*, 3177-3185.

66. Jorgensen, W. L.; Maxwell, D. S.; Tirado-Rives, J. Development and testing of the OPLS all-atom force field on conformational energetics and properties of organic liquids. *J. Am. Chem. Soc.* **1996,** *118*, 11225-11236.

67. Dang, L. X. Mechanism and thermodynamics of ion selectivity in aqueous solutions of 18-crown-6 ether: a molecular dynamics study. *J. Am. Chem. Soc.* **1995,** *117*, 6954-6960.

68. Berendsen, H.; Grigera, J.; Straatsma, T. The missing term in effective pair potentials. *J. Phys. Chem.* **1987,** *91*, 6269-6271.

69. Jorgensen, W. L.; Chandrasekhar, J.; Madura, J. D.; Impey, R. W.; Klein, M. L. Comparison of simple potential functions for simulating liquid water. *J. Chem. Phys.* **1983,** *79*, 926-935.

70. Joung, I. S.; Luchko, T.; Case, D. A. Simple electrolyte solutions: Comparison of DRISM and molecular dynamics results for alkali halide solutions. *J. Chem. Phys.* **2013,** *138*, 044103.

71. Jiang, H.; Mester, Z.; Moultos, O. A.; Economou, I. G.; Panagiotopoulos, A. Z. Thermodynamic and transport properties of H_2O + NaCl from polarizable force fields. *J. Chem. Theory Comput.* **2015,** *11*, 3802-3810.

72. Mester, Z.; Panagiotopoulos, A. Z. Temperature-dependent solubilities and mean ionic activity coefficients of alkali halides in water from molecular dynamics simulations. *J. Chem. Phys.* **2015,** *143*, 044505.

73. Abascal, J.; Fernandez, R. G.; MacDowell, L.; Sanz, E.; Vega, C. Ice: A fruitful source of information about liquid water. *J. Mol. Liq.* **2007,** *136*, 214-220.

74. Smith, D. E.; Dang, L. X. Computer simulations of NaCl association in polarizable water. *J. Chem. Phys.* **1994,** *100*, 3757-3766.

75. Gee, M. B.; Cox, N. R.; Jiao, Y.; Bentenitis, N.; Weerasinghe, S.; Smith, P. E. A Kirkwood-Buff derived force field for aqueous alkali halides. *J. Chem. Theory Comput.* **2011,** *7*, 1369-1380.

76. Moučka, F.; Lísal, M.; Smith, W. R. Molecular simulation of aqueous electrolyte solubility. 3. Alkali-halide salts and their mixtures in water and in hydrochloric acid. *J. Phys. Chem. B* **2012,** *116*, 5468-5478.

77. Mester, Z.; Panagiotopoulos, A. Z. Mean ionic activity coefficients in aqueous NaCl solutions from molecular dynamics simulations. *J. Chem. Phys.* **2015,** *142*, 044507.

78. Hub, J. S.; de Groot, B. L.; Grubmüller, H.; Groenhof, G. Quantifying artifacts in Ewald simulations of inhomogeneous systems with a net charge. *J. Chem. Theory Comput.* **2014,** *10*, 381-390.

79. Young, J. M.; Panagiotopoulos, A. Z. System-size dependence of electrolyte activity coefficients in molecular simulations. *J. Phys. Chem. B* **2018,** *122*, 3330-3338.

80. Chase, M. NIST-JANAF Thermochemical Tables (J. Phys. Chem. Ref. Data Monogr. 9). Woodbury, NY: AIP: 1998.

81. Young, J. M.; Tietz, C.; Panagiotopoulos, A. Z. Activity coefficients and solubility of $CaCl_2$ from molecular simulations. *J. Chem. Eng. Data* **2020,** *65*, 337-348.

82. Bennett, C. H. Efficient estimation of free energy differences from Monte Carlo data. *J. Comput. Phys.* **1976,** *22*, 245-268.

83. Allen, M. P.; Tildesley, D. J., *Computer simulation of liquids*. Oxford university press: 2017.

84. Abraham, M. J.; Murtola, T.; Schulz, R.; Páll, S.; Smith, J. C.; Hess, B.; Lindahl, E. GROMACS: High performance molecular simulations through multi-level parallelism from laptops to supercomputers. *SoftwareX* **2015,** *1*, 19-25.

85. Nosé, S. A unified formulation of the constant temperature molecular dynamics methods. *J. Chem. Phys.* **1984,** *81*, 511-519.

86. Hoover, W. G. Canonical dynamics: Equilibrium phase-space distributions. *Physical review A* **1985,** *31*, 1695.

87. Davies, C. W. 397. The extent of dissociation of salts in water. Part VIII. An equation for the mean ionic activity coefficient of an electrolyte in water, and a revision of the dissociation constants of some sulphates. *JournalSeek* **1938,** 2093-2098.

88. Uematsu, M.; Frank, E. Static dielectric constant of water and steam. *J. Phys. Chem. Ref. Data* **1980,** *9*, 1291-1306.

89. Robinson, R. A.; Stokes, R. H., *Electrolyte solutions*. Courier Corporation: 2002.

90. Sun, L.; Liang, X.; Solms, N. v.; Kontogeorgis, G. M. Analysis of some electrolyte models including their ability to predict the activity coefficients of individual ions. *Ind. Eng. Chem. Res.* **2020,** *59*, 11790-11809.

91. Maribo-Mogensen, B.; Thomsen, K.; Kontogeorgis, G. M. An electrolyte CPA equation of state for mixed solvent electrolytes. *AIChE J.* **2015,** *61*, 2933-2950.

92. Shilov, I. Y.; Lyashchenko, A. K. The role of concentration dependent static permittivity of electrolyte solutions in the Debye–Huckel theory. *J. Phys. Chem. B* **2015,** *119*, 10087-10095.

93. Lebowitz, J.; Percus, J. Mean spherical model for lattice gases with extended hard cores and continuum fluids. *Phys. Rev.* **1966,** *144*, 251.

TOC GRAPHIC